Title
ANGLE-RESOLVED PHOTEMISSION STUDIES OF THE VALENCE BAND STRUCTURE OF STEPPED CRYSTAL SURFACES: Cu(S)-D(lll)x(100)J

Author
Davis, R.F.

Publication Date
1981-08-01

LBL-8511
Preprint

Lawrence Berkeley Laboratory
UNIVERSITY OF CALIFORNIA

Materials & Molecular Research Division

Submitted to Physical Review B

ANGLE-RESOLVED PHOTOEMISSION STUDIES OF THE VALENCE BAND STRUCTURE OF STEPPED CRYSTAL SURFACES: Cu(S)-[3(111)x(100)]

R.F. Davis, R.S. Williams, S.D. Kevan,
P.S. Wehner, and D.A. Shirley

August 1981

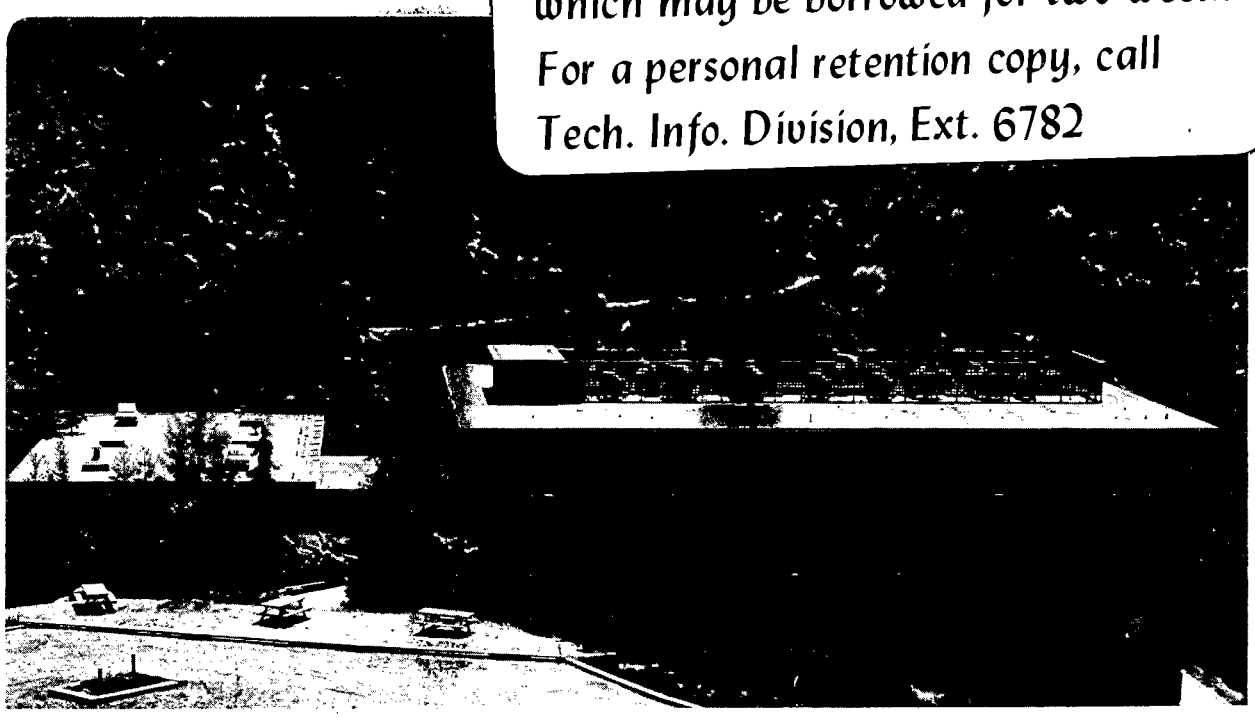

Prepared for the U.S. Department of Energy under Contract W-7405-ENG-48

DISCLAIMER

LBL-8511

ANGLE-RESOLVED PHOTOEMISSION STUDIES OF THE VALENCE BAND STRUCTURE OF STEPPED CRYSTAL SURFACES: Cu(S)-[3(111)x(100)]

R.F. Davis, R.S. Williams, S.D. Kevan,
P.S. Wehner, and D.A. Shirley

Materials and Molecular Research Division
Lawrence Berkeley Laboratory
and
Department of Chemistry
University of California
Berkeley, California 94720

August 1981

This work was supported by the Director, Office of Energy Research, Office of Basic Energy Sciences, Chemical Sciences Division of the U.S. Department of Energy under Contract No. W-7405-ENG-48. It was performed in part at the Stanford Synchrotron Radiation Laboratory, which is supported by the NSF Grant No. DMR 77-27489, in cooperation with the Stanford Linear Accelerator Center.

ANGLE-RESOLVED PHOTOEMISSION STUDIES OF THE VALENCE BAND STRUCTURE OF STEPPED CRYSTAL SURFACES: Cu(S)-[3(111)x(100)]

R.F. Davis,* R.S. Williams,† S.D. Kevan,‡
P.S. Wehner,§ and D.A. Shirley

Materials and Molecular Research Division
Lawrence Berkeley Laboratory
and
Department of Chemistry
University of California
Berkeley, CA 94720

ABSTRACT

Angle-resolved photoemission spectra are reported for the stepped Cu(211) face in the photon-energy range 9 eV $\leq h\nu \leq$ 34 eV. The valence-band (VB) spectra are interpreted in terms of a direct-transition model for bulk photoemission. Determination of VB dispersion relations and assignment of the bands are aided by use of selection rules involving the transmitted radiation vector potential and several different experimental geometries. The major results are: (1) it is possible to determine experimental VB dispersion relations for non low-Miller-index directions; (2) VB dispersion relations for stepped Cu(211) show excellent agreement with bulk valence bands interpolated along the [211] direction; (3) the quasi-free electron model describes photoelectron dispersion relations, but the one-electron

---

* Address after Oct. 1, 1981: Polaroid Corporation, Waltham, MA 02154

† Present address: Department of Chemistry, University of California, Los Angeles, CA 90024.

‡ Present address: Bell Laboratories, Murray Hill, NJ 07974.

§ Present address: Tennessee Eastman Company, Kingsport, TN 37662.

bulk conduction bands do not; and (4) there is no evidence for band-gap photoemission into a gap that is predicted in the bulk conduction band structure ca. 10 to 14 eV above the Fermi level: the peaks show dispersion through this energy range. It is concluded that the unusual structure of the stepped surface does not significantly perturb the bulk electronic structure near the surface.

I. INTRODUCTION

Detailed angle-resolved photoemission (ARP) studies of the face-centered cubic (FCC) metals copper,[1-5] silver,[6,7] gold,[8-11] nickel,[12] palladium,[13] platinum,[8,14] and iridium[15] have shown that the peak structures in photoelectron energy distribution curves (EDCs) arise mainly from energy- and crystal momentum-conserving direct electronic transitions near or at the surface. Consequently, by combining the photon energy-variability of synchrotron radiation with a normal electron emission geometry, these studies[1,2,4,6,8,9,12-15] have resulted in the determination of empirical bulk valence-band dispersion relations along $\vec{k}_\perp$ (the surface perpendicular or normal component of the crystal momentum $\vec{k}$) with remarkable success. However, in each case, the surface studied was a low-Miller-index plane [i.e., (100), (110), or (111)]. These studies yielded experimental energy bands along high-symmetry lines in k-space, permitting ready comparisons to published theoretical band structure calculations.

In this paper, we report angle-resolved normal photoemission (ARNP) valence-band studies of the Cu(211) face. These experiments directly address a number of important problems in photoemission from metals. The complexity of ARNP from (110) and (100) faces[16] relative to (111) suggests that a detailed understanding of ARNP from still lower symmetry faces--such as (211)--might be very difficult or impossible. This hypothesis has several origins. First, low k-space symmetry induces a complete non-degeneracy of the energy levels at most reduced

k points along the [211] line. Secondly, the relatively large surface unit cell of high-index faces gives rise to a set of small two-dimensional reciprocal lattice vectors which may induce surface umklapping of photoelectrons with higher cross-section than on unreconstructed low-index faces.[17] Furthermore, like many high-index faces of the Group VIII and I-B metals oriented in the [01$\bar{1}$] crystallographic zone,[18] the clean Cu(211) surface develops a stable stepped structure after annealing. The electronic structure of stepped and kinked surfaces is of considerable interest because the step and/or kink atoms on such surfaces are believed to influence surface reactivity.[19] Although there is some experimental[20] and theoretical[21] evidence that enhancement of surface reactivity may arise more from steric effects due to step-adsorbate geometry than from any particular electronic-structural property of the steps, some theoretical calculations predict, in certain cases, substantially different electronic environments for step or kink atoms relative to atoms on planar surfaces.[22,23]

An important result of this work concerns a conduction band gap along [211], which affects the band structure near, but not at, the Brillouin zone boundary. As demonstrated below, our data show essentially no evidence for the "band-gap photoemission" process discussed by previous workers,[17,24,25] Rather, we show that through a combination of different radiation polarization directions and energies ($h\nu$), a detailed understanding of the photoemission process from Cu(211) is obtained within the framework of the direct-transition

model using a quasi-free electron final-state band structure. Furthermore, although the low symmetry of Cu(211) does indeed introduce a great deal of structure to the EDCs, it also allows us to investigate the symmetry and dispersion properties of each individual valence band.

In Section II, we discuss experimental procedures. Section III describes the results within a bulk direct-transition framework. Section IV contains a general discussion, and Section V gives a summary.

II. EXPERIMENTAL

A high purity single crystal slab of Cu was cut and mechanically polished to within $\pm 0.5^\circ$ of the (211) plane (19.5° from [111] in the [01$\bar{1}$] zone), with a mean surface roughness of 1-μm. After a chemical polish,[26] the crystal was installed in an ultrahigh-vacuum chamber (base pressure ~3 x 10^{-10} torr) for *in situ* preparation and characterization of the Cu(S)-[3(111)x(100)] stepped surface,[18,27] an ideal segment of which is depicted in Fig. 1. Preparation was accomplished by repeated cycles of Ar^+ sputtering, followed by annealing at ~875K. Immediately preceding the ARP experiments, the resulting surface was monitored by Auger electron spectroscopy (AES) for cleanliness and low energy electron diffraction (LEED) for crystallographic order, giving rise to AES impurity signals characteristic of $\lesssim$0.05 monolayer contamination and LEED patterns (with extremely sharp and intense spots) characteristic of the stable step surface structure. As shown in

Fig. 1, the (211) surface consists of (111) oriented terraces with three inequivalent atomic rows (labeled A, B, and C) that are parallel to the $[01\bar{1}]$ direction, and monatomic steps of (100) orientation. The only symmetry element that this surface contains is the $(01\bar{1})$ mirror plane which cuts through the surface perpendicular to the atomic rows.

The photoemission measurements were performed on the 8° branch of Beam Line I (BL I-2) at the Stanford Synchrotron Radiation Laboratory with the incident radiation highly polarized (> 97%) in the horizontal plane and in the energy range 9 eV $\leq h\nu \leq$ 34 eV. Our ARP instrument, described elsewhere,[28] employs a rotatable 5.40 cm mean radius hemispherical analyzer with an angular acceptance of ±3°. In these measurements, the energy resolution (monochromator plus electron analyzer) varied from ca. 0.12 eV to ca. 0.25 eV (FWHM) at the lower and upper photon energies, respectively.

As shown in Fig. 2, experiments were done with two different normal emission geometries, conversion between which was achieved by azimuthal rotation of the crystal about its normal ($\vec{n}$) by 90°. For both orientations, the incident radiation vector potential ($\vec{A}$) was confined to the plane of incidence, and the photoemission direction ($\vec{p}$) was confined to the surface normal ([211]). In orientation I [Fig. 2(a)], $\vec{A}$ lies in a crystallographic plane perpendicular to the $(01\bar{1})$ mirror plane (M) with $\phi_A = 0°$, whereas in orientation II [Fig. 2(b)], $\vec{A}$ lies in M (M is the plane of incidence in this case) with $\phi_A = 270°$. The angle θ_A (between $\vec{n}$ and $\vec{A}$) could be varied between 10° and 45° in either ϕ_A azimuth by coupling analyzer and crystal polar rotations,

but the majority of measurements were performed with $\theta_A = 30^\circ$. At this angle, $\vec{A}$ is aligned with the [110] direction in orientation I, and is ~ 5° from alignment with [100] in orientation II. In situ polar crystallographic alignment (± 1°) was achieved using a He-Ne laser, and the azimuthal orientation (± 3°) was determined from LEED patterns. We shall henceforth refer to orientations I and II as simply (I) and (II), respectively.

Typical EDCs for the entire energy range are shown in Fig. 3 for both orientations and $\theta_A = 30^\circ$. Only 24 spectra are plotted here, for brevity. Our interpretation is based on a total of 82 spectra. In each spectrum, the Fermi level (E_F) was determined as $(dJ/dE)_{max.}$, i.e., the point of maximum derivative of photoelectron intensity with respect to energy, in the region near the onset of the s-p plateau. Because of relatively low intensity (J), this procedure became progressively more difficult in the higher photon energy region ($h\nu \gtrsim 20$ eV), particularly for the spectra taken with the sample in (I). Nevertheless, the work functions derived from E_F placement and analyzer reference voltages showed an rms scatter of only ± 35 meV for the entire data set.

III. DIRECT-TRANSITION MODEL FRAMEWORK

The spectra shown in Fig. 3 clearly indicate that (a) the low symmetry of the (211) face introduces complexity to the valence band peak structure relative to the spectra of low-index Cu faces, and (b) there is a strong dependence on radiation polarization, as the

only difference between the two orientations is the direction of $\vec{A}$ relative to the crystallographic axes. The behavior of the various contributions to the spectra, which can be identified and shown to disperse as a function of photon energy, is highly indicative of bulk direct-transition processes, particularly because $\vec{k}_{\parallel}$ (surface component of momentum) is zero for normal emission. This behavior is demonstrated by the structure plots for both orientations, shown in Fig. 4. The circles represent strong peak (closed circles) or weak feature (open circles) energy positions relative to E_F for the range of photon energies used. The distinction between strong and weak features is somewhat artificial--indicative of greater peak position uncertainty but not necessarily of relative peak intensity--because the complexity of the spectra gives rise to substantial peak convolution. For example, the intensity of the most tightly bound peak in (II) appears to be weak for 14 eV $\leq h\nu \leq$ 16 eV and negligible for $h\nu <$ 14 eV, but this is probably because the peak is hidden behind the tail region of the second most tightly bound feature, which is an intense peak at these photon energies. The connecting lines on the plots in Fig. 4 have no significance other than to join and map the individual structures as a function of $h\nu$. The reproducibility between the two sets of plots [(I) and (II)] is excellent, as equivalent peaks which are found in spectra for both orientations (at a given $h\nu$) are typically separated by 0.04 eV or less.

In the normal emission geometry, peak energy dispersion with $h\nu$ as shown in Fig. 4 can only occur from direct transitions at reduced

k-points which yield photocurrent in normal emission, i.e., those which either are part of the [211] direction crystal momentum space or which are in other directions but can excite transitions that result in normal emission via surface umklapp processes.[17,29] Normal emission from [211] line initial states could arise from primary Mahan cones[29] or from electrons excited away from [211] that reach the detector via surface umklapps (secondary cones). We proceed, below, to set up a bulk band structure framework[30] with which to interpret the data represented in Figs. 3 and 4, and we show that excellent agreement between experiment and theory is obtained if (a) only $\vec{k}_{\perp}$-conserving transitions from [211] initial states are assumed to occur, and (b) only one final state band is important in transmitting photocurrent to the analyzer (i.e., no secondary Mahan cones contribute peak structures).

A. Characteristics of Cu[211] Bands

The irreducible portion of k-space lying along [211], all of which is contained in the $(01\bar{1})$ plane, is shown as the dashed line in Fig. 5. The point B = (3/4,3/8,3/8) (in units of $2\pi/a$, which will be used throughout this work) is equivalent to D = (-1/4,-5/8,-5/8), both being at the Brillouin zone boundary. Although these points have no other significance or special symmetry properties it is useful to designate them as B and D. The group of the $\vec{k}$-vector (the point group C_s) corresponding to points along [211] ($\Gamma \rightarrow B$, $D \rightarrow X$) contains only the identity element (E) and the $(01\bar{1})$ mirror plane (σ_h). Thus,

electronic states lying on the [211] crystal momentum axis may be symmetry classified as either even or odd (A' or A", respectively, in C_s) with respect to reflection through the mirror plane.

The energy bands for Cu were generated for the [211] crystal momentum line using Smith's parameterization[31] (with minor modification of several parameters) of the Hodges, Ehrenreich, and Lang interpolation scheme.[32] Although the fitting procedure considers only the occupied bands, this interpolation scheme reproduced the energy bands calculated by Janak, et al.[33] quite well up to E^F = +20 eV (E^F is energy relative to E_F). Thus, the resulting band structure shown in Fig. 6 should give a fairly good representation of both the valence bands and the conduction bands up to +20 eV. Energy bands were also calculated using interpolation parameters derived from the critical point eigenvalues of Janak, et al.,[33] and from experimental energy level positions based on Cu(111) and Cu(100) studies by Knapp, et al.[2] and Cu(110) studies by Thiry, et al.,[4] but neither of these two calculations agreed as well with our data as the one which utilized Smith's parameterization, which is based on Burdick's[34] augmented plane wave (APW) calculation. From careful inspection of the eigenvectors in our calculation, we determined the irreducible representations (A' or A") of the first nine bands at each k point, and have labeled the bands shown in Fig. 6 accordingly. We found it useful to label the bands of each type separately according to increasing band index, but this has no group-theoretical significance. It does, however, remove ambiguities caused by band crossings. Of the

six valence bands, four have A' symmetry, while two of the three lowest conduction bands also have A' symmetry. As shown, the band structure reveals a gap in the conduction bands between A_5' and A_6' from about 10.2 eV to 13.0 eV above E_F. In principle, a conduction band gap has implications for ARP if it involves the photoemission final states.[17,24,25] Although the precise location and width of the gap are not necessarily accurate in our calculation, the existance of a gap near E^F = 12 eV is guaranteed by symmetry considerations.

B. Photoemission Properties of Cu[211] Bands

Hermanson[35] has discussed the polarization selection rules for photoemission normal to low-index faces of cubic crystals, and there have been several experimental studies of these polarization effects.[2,36] In this study, we have incorporated two different polarization geometries to investigate the importance of these effects for a stepped crystal face, for which the symmetry properties are simple. Polarization selection actually reduces considerably the problem of determining dispersion relations for each individual valence band in Cu(211), as will be discussed below. The selection rules governing ARNP from Cu(211) are summarized in Table I. The photoemission final state must belong to the A' (symmetric) irreducible representation because operations which leave the crystal invariant should not affect the electronic state sampled by the detector. Thus, in order for a transition to be allowed, the irreducible representation of a particular initial state must be contained in the transition

operator $\vec{A}\cdot\vec{p}$. Referring to Fig. 2 and Table I, the component of $\vec{A}$ along [01$\bar{1}$] (orthogonal to M) can excite A" initial states (A_1'' or A_2''), while components along [211] and [$\bar{1}$11] (lying in M) excite only A' (A_1' through A_4') initial states. Thus, for the geometries shown in Fig. 2, the spectra accumulated in (I) may arise from A' → A' and A" → A' transitions, with $|A_x/A_z| = 0.6$ at $\theta_A = 30°$. On the other hand, the spectra from (II), with $A_x = 0$, should arise from A' initial state bands only. Careful inspection of relative peak intensities in the spectra (Fig. 3) indicates a qualitative verification of these selection rules for Cu(211) direct transitions. Aided by direct comparison of theoretical and experimental band structures (vide infra), we have labeled the structure plots in Fig. 4 according to the initial states involved in the transitions. Symmetry effects in our spectra will be discussed at greater length in the next section.

In consonance with previous studies,[6,8,9,14] the photoemission final states were taken partly to be A' conduction band components which are derived from the empty lattice conduction band(s) that would be involved in [211] primary Mahan[29] cone emission. Between Γ and B, there are no unbound primary cone components in the energy range excitable with $h\nu \leq 34$ eV, as the smallest reciprocal lattice vector involved in a primary cone transition $\vec{k}_i \rightarrow \vec{k}_i - \vec{G}$ (in the empty lattice approximation) would be $\vec{G} = (4,2,2)$; this would require $h\nu > 170$ eV at $\vec{k}_i = B$. However, there is primary emission in our energy range from final states between D and X, shown in Fig. 6 as the regions of A_5' and A_6' highlighted by filled circles. These states

are derived from $\vec{G} = (\bar{1},\bar{1},\bar{1})$. In the band gap regions, 9.0 eV $\leq E^F \leq$ 14.0 eV and $E^F \geq$ 26.5 eV, the final states were derived from $E^F(\vec{k}) = (\hbar^2/2m^*)|\vec{k} - \vec{G}|^2 + V_0^F$, with $\vec{G} = (\bar{1},\bar{1},\bar{1})$. These states are shown in Fig. 6 as the two dashed curves connecting A_5' with A_6' and extending beyond A_6'. The parameters m* (reduced mass) and V_0^F (inner potential) were calculated from a fit of this free-electron-like dispersion relation to the regions of A_5' and A_6' highlighted by filled circles in Fig. 6, yielding $m^* = 0.89\ m_e$ and $V_0^F = -8.0$ eV. This value of m* is consistent with that determined experimentally by Knapp, et al.[2] for the Δ_1 conduction band in Cu(001) [$(m^*/m_e) = 0.90 - 0.94$]. Using the measured[37] value for the Cu(211) work function (Φ = 4.53 eV), we obtain $V_0^V = -12.5$ eV (V_0^V is the vacuum-referenced inner potential) for our final-state band, reasonably consistent with the value determined from LEED studies[38] of Cu(001) ($V_0^V = -13.5$ eV). In contrast to several previous studies (see, e.g., Ref. 14), this Cu(211) quasi-free electron final-state dispersion relation was used without modification.

In Fig. 7, we show a comparison of our empirically derived valence band positions (symbols) with the interpolated dispersion relations (lines) for all six valence bands along [211]. The arrows at E_F indicate k values for which A_4' intersects the Fermi surface (from de Haas van Alphen data[39]). The empirical bands in Fig. 7 represent the combined data of (I) and (II) (Figs. 3 and 4). If a peak appeared in both orientations, the mean value was used to determine the band position. The points in Fig. 7 were positioned in the standard way[30]

by determining $\vec{k}_i$ from the final-state band highlighted in Fig. 6. Then, for each valence band, the points were fitted to a smooth curve, yielding empirical dispersion relations. These are tabulated in Table II for selected values of $\vec{k}_i$ within the region of [211] k-space sampled by the 9 eV $\leq h\nu \leq$ 34 eV radiation [$\vec{k}_i$ between (-0.14,-0.57,-0.57) and (0.42,-0.29,-0.29)]. Considering both the complexity of the Cu(211) EDCs and the possible inaccuracies associated with our interpolation scheme calculation,[32] the theoretical and experimental bands generally agree quite well and both agree with the Fermi surface data.[39] The only feature in the EDCs which does not appear to arise from direct transitions is a weak shoulder at $E^F = -2.30 \pm 0.02$ eV in the spectra for 9 eV $\leq h\nu \leq$ 16 eV. It is reasonable to attribute this nondispersive feature to the d-band edge in the density of states. A similar feature was noted in silver,[6] gold,[8] and platinum[8] ARNP spectra.

We can describe the "agreement" between experiment and interpolation theory quantitatively by calculating $\Delta E = E^F(\text{expt.}) - E^F(\text{int.})$ for each energy level listed in Table II, where $E^F(\text{int.})$ is the interpolated energy position. The results are listed in Table III, along with similar (theoretical) numbers reported by Hodges, et al.[32] for a general comparison of interpolated Cu bands with Burdick's[34] APW calculation. The theoretical ΔE values represent the general limitations of the interpolation method and thus are lower bounds on the size of ΔE values that might reasonably be expected for these Cu(211) studies. Conversely, experimentally derived ΔE values that are smaller

than those of Hodges, et al.[32] are not meaningful. By this criterion, the differences between the interpolated and experimental band structures are negligible for all bands except A_1' and A_4'. Inspection of the dispersion relations in Fig. 7 indicates that the greater deviations in A_1' and A_4' arise from the region of k-space near $\vec{k}_i$ = (0.38,-0.31,-0.31); i.e., halfway between D and X. The group velocity ($\vec{v}_g$) of the A_1' band approaches zero near E^F = -5.40 eV (expt.) and -5.68 (int.), yielding a value of ΔE (0.28 eV) that is consistent with deviations observed in the $v_g = 0$ region of the lowest s-band on low-index faces of Cu.[2,4] Our measurements indicate that A_4' approaches $v_g = 0$ in this $\vec{k}_i$ region with E^F = -2.65 eV while the interpolation value is -2.34 eV, yielding ΔE = -0.31 eV. This is somewhat puzzling, because the experimental position of the uppermost s-p band on low-index faces[2,4] agrees well with the APW theory[33] along Σ, Λ, or Δ. Thus, the discrepancy observed in A_4' may well result from an associated larger error in its interpolated dispersion relation relative to the other bands. This is supported by the existence of large experiment - interpolation deviations in A_4' band energies throughout most of the region of the Brillouin zone sampled by our experiments. We cannot, however, completely rule out the possibility that transitions occur at or near Γ (i.e., transitions like $\Gamma_{12} \rightarrow \Gamma_{2'}, \Gamma_{15}, \Gamma_{25'}$), where the empty lattice final states are highly degenerate and the valence band density of states is large. This would yield peak structure at or near E^F = -2.85 eV. The average of $E^F(\Gamma)$ and E^F(0.38,-0.31,-0.31), -2.60 eV, is very close to the observed A_4'

band position at $\vec{k}_i$ = (0.38,-0.31,-0.31). However, transitions at Γ are unlikely to yield the considerable intensity observed near E^F = -2.60 eV in the EDCs, because they produce photoelectrons with group velocities in directions other than [211]; i.e., they are secondary Mahan cones in normal emission, and secondary emission is expected to be negligible at the relatively high ($h\nu \gtrsim 30$ eV) photon energies required for Γ transitions. This explanation of the deviation in A_4' near the minimum also does not address the deviations elsewhere along D - X.

Other than the shapes of the A_1'' and A_2'' experimental bands (especially near $\vec{k}_i$ = D, where the $A_2'' - A_1''$ splitting is smaller than expected), the measured dispersion relations agree very well with the interpolated bands. Deviations are about as large as the errors expected in the interpolated bands alone (see Table III). This represents the most significant result of this work.

IV. DISCUSSION

A bulk direct-transition framework has been set up and shown to fit the Cu(211) data quite well. Now, the results will be discussed with particular emphasis on: (a) symmetry properties of the Cu(211) EDCs, and (b) final-state structure and the absence of band-gap photoemission.

A. Symmetry Properties

In Fig. 8, Cu(211) spectra ($\theta_A = 30^\circ$) at several photon energies are directly compared for the two orientations, (I) and (II). The EDCs in each set of curves are normalized to the most intense feature. Throughout the data range, the majority of peak intensity in (I) (where direct transitions from A" and A' states are allowed) arises from A_1', A_2', A_1'', and A_2'', whereas (II) (only A' states allowed) is dominated by photoexcitation from A_1', A_2', and A_4'. Relative intensity and dispersion characteristics of each valence band feature will be discussed separately, beginning with the uppermost band.

(1) A_4'. Below $h\nu = 19$ eV, A_4' clearly dominates the s-p plateau region of the spectra in (II), while no peak is observed there in (I). The s-p plateau, which arises from indirect transitions, is larger in (II) than in (I) over most of the photon energy range. This is shown by the top curve in Fig. 9, where $R_{21} = J(II)/J(I)$ is plotted for the s-p region, and may be an indication that indirect transitions also follow a polarization selection rule in photoemission. If so, the s-p plateau arises largely from indirect transitions at k points which have point group symmetry no lower than that of the [211] line, i.e., those lying in the $(01\bar{1})$ plane. However, a selection rule for indirect transitions is only rigorously valid if there always exists a phonon of the correct symmetry[40] which can couple with the $\vec{k}$ vector of the electron in the photoexcitation transition. Indirect transitions undoubtedly arise from d bands also, but this is masked by the large direct-transition intensity in the d-band region. Between $h\nu = 9$ and

19 eV, A_4' disperses from E^F = -0.23 to -1.78 eV in (II). At $h\nu$ = 20 eV, the A_4' intensity in (II) has moved into coincidence with part of the A_2'' peak centered at E^F = -2.30 eV, making a definitive peak position assignment of A_4' impossible and giving the misleading appearance of a resonance in the A_2'' peak in this energy range (cf. $h\nu$ = 22 eV in Fig. 8). At $h\nu$ = 25 eV and E^F = -2.42 eV, A_4' again appears as a separate structure in (II), splitting away from A_2'' on the higher binding energy side. Additionally, A_4' appears in (I) for the first time at $h\nu$ = 26 eV with E^F = -2.51 eV. We note that the large intensity of the A_4' peak for $h\nu \geq 25$ eV is related to the large amount of d character that its wave function picks up near $\vec{k}_i$ = (0.38,-0.31,-0.31) because it mixes strongly with the uppermost d band. Thus, A_4' is the dominant feature in the spectrum for (II) at $h\nu$ = 34 eV (see Fig. 8) with E^F = -2.55 eV, and is clearly discernable in (I) for $h\nu \geq 26$ eV. In (II) and (I), respectively, A_4' continues to disperse downward at $h\nu$ = 26 eV with E^F = -2.46 and -2.51 eV, to E^F = -2.68 and -2.70 eV at $h\nu$ = 30 eV, where it reaches a band minimum. It disperses upward toward E_F for $h\nu > 30$ eV in both orientations.

(2) A_2''. A_2'' apparently contributes intensity to spectra in both orientations throughout the energy range studied. Possible causes for the large intensity in the A_2'' region of the EDCs in (II), where it is symmetry forbidden, can be discussed. First, A_2'' is convoluted with A_4' completely for 19 eV < $h\nu$ < 25 eV and partially for several electron volts on either side of this range, giving the misleading appearance of a large A_2'' intensity. In addition, the

intensity of the A_2'' peak was found to be extremely sensitive to the azimuthal angle ϕ_A; thus, some of its intensity in (II) must arise from the relatively large ($\pm 3^\circ$) uncertainty in ϕ_A, as well as from the finite ($\pm 3^\circ$) geometric half-angular acceptance of the analyzer. In other words, if A_2'' intensity is very sensitive to ϕ_A, then it appears in our spectra for (II) because $\vec{A}$ has a small component along the x-axis ($\perp$ to M) because of the angular uncertainty in ϕ_A. Furthermore, while density-of-states (DOS) photoemission does not play a dominant role in our spectra, it yields a weak shoulder ($E^F = -2.30$ eV) in the spectra for $h\nu \leq 16$ eV. A photoelectron sampling depth argument suggests that DOS emission should be enhanced at higher photon energies.[41] Thus, although apparently absent from the spectra for $h\nu > 16$ eV, it is undoubtedly hidden beneath direct-transition intensity from A_2'' in (I) and may account for a large part of the intensity of A_2'' in (II). The empirical A_2'' band is extremely flat, with an average energy of $E^F = -2.40 \pm 0.08$ eV. Thus, it could easily coincide with a DOS peak at -2.30 eV. But, if polarization selection is valid for DOS features, the DOS intensity in (II) cannot arise from a one-dimensional DOS because it would arise almost entirely from symmetry-forbidden A_2'' states, i.e., it must be from the three-dimensional DOS.

The energy-dispersive characteristics of A_2'' in both orientations are similar: $E^F = -2.60$ eV at $h\nu = 11$ eV, dispersing up to $E^F = -2.33$ eV at $h\nu = 19$ eV; it remains relatively flat until $h\nu = 23$ eV where it begins to move away from E_F, moving to $E^F = -2.41$ eV at

$h\nu = 27$ eV. Above $h\nu = 27$ eV, A_2'' rises, reaching $E^F = -2.27$ eV at $h\nu = 34$ eV.

(3) A_1''. This is the most intense feature in (I), but it is essentially absent from (II), appearing only as a weak shoulder at most photon energies in the latter orientation. For this reason, definitive empirical dispersion relations for A_2' and A_3' near $\vec{k}_i = (0.38,-0.31,-0.31)$ could be determined. In (I), A_1'' masks the weaker A_2' feature for $h\nu > 23$ eV and the much weaker A_3' feature for $h\nu > 18$ eV. But, in (II) the A_1'' peak is small below $h\nu = 22$ eV and absent above, allowing the band positions of A_3' and A_2' to be determined. This is another important result of this work: symmetry considerations may be used to effectively "turn off" bands and determine individual band dispersion relations along what would otherwise be considered a complicated direction in k-space. The A_1'' peak can be clearly seen at low photon energies, starting with $h\nu = 12$ eV and $E^F = -2.78$ eV in (II) and $h\nu = 13$ eV, $E^F = -2.84$ eV in (I). At $h\nu = 12$ eV, A_2'' obscures the A_1'' peak in (I) (the empirical $A_1'' - A_2''$ splitting in this region is only about 0.25 eV). In (II), where it is symmetry forbidden, A_1'' becomes relatively weaker with increasing energy. In the range $20 \text{ eV} \leq h\nu \leq 22$ eV, A_1'' is visible in (II) as a weak shoulder on the low binding energy side of the intense A_2' direct-transition peak, with $E^F = -3.42$ eV at $h\nu = 22$ eV (cf. Fig. 8). In (I), where it is symmetry allowed, A_1'' moves from $E^F = -2.84$ eV at $h\nu = 13$ eV (where it is still smaller than A_2''), to $E^F = -3.54$ eV at $h\nu = 27$ eV, becoming the dominant feature in the spectra for $h\nu \geq 15$ eV.

Above $h\nu = 27$ eV, A_1'' moves toward E_F again, reaching $E^F = -3.39$ eV at $h\nu = 34$ eV. It actually crosses the A_3' and A_2' dispersion relations; this can be seen in Fig. 8 in the spectra for $h\nu = 28$ eV, where $E^F(A_1'') = -3.53$, $E^F(A_2') = -3.46$, and $E^F(A_3') = -3.28$ eV.

(4) A_3'. This transition is apparently weak, appearing as a shoulder on the low binding energy side of A_2' in both orientations. In (I) it is seen at $h\nu = 13.0$, 13.5, 17.0, and 18.0 eV with energies in the range -3.74 eV $\leq E^F \leq -3.61$ eV. In (II), where A_1'' is not a strong feature, A_3' is observed in the range 17 eV $\leq h\nu \leq$ 29 eV with $E^F = -3.79$ and -3.28 eV at the low and high photon energy limits of this range, respectively.

(5) A_2'. This band contributes the largest intensity to the EDCs over most of the photon energy range in (II), and in (I) is a large peak although obscured for $h\nu \geq 24$ eV by the stronger symmetry allowed A_1'' transition. The A_2' onset is at $h\nu = 11$ and 13 eV with energies $E^F = -3.93$ and -3.81 eV in (II) and (I), respectively. By $h\nu = 13.5$ eV, A_2' is the dominant feature in (II), with $E^F = -3.89$ eV. It moves to $E^F = -4.01$ eV at $h\nu = 15.0$ eV, then disperses upward for $h\nu > 15$ eV, reaching $E^F = -3.40$ at $h\nu = 30$ eV. Finally, it is found at $E^F = -3.46$ at $h\nu = 34$ eV. In (I), A_2' disperses upward for $h\nu > 13$ eV, until it is obscured by the A_1'' peak at $h\nu = 24$ eV near the energy where these two bands cross.

(6) A_1'. A relatively large peak is observed from A_1' in both orientations and for $h\nu > 13.5$ eV. It appears to be somewhat weaker in (II) relative to (I) than would be expected by symmetry considerations,

but this is undoubtedly because it is obscured by the strong A_2' transition below $h\nu = 16$ eV. However, it is still clearly seen in each orientation starting at $h\nu = 13.5$ and 14.0 eV, with $E^F = -4.16$ and -4.21 eV, in (I) and (II), respectively. From there, A_1' disperses downward in both orientations, reaching a band minimum with $E^F = -5.42$ eV at $h\nu = 29$ eV. It would be somewhat difficult to determine the A_1' band position accurately for 14 eV $\leq h\nu \leq$ 18 eV without the aid of the spectra in (I). These spectra (cf. $h\nu = 14$ and 16 eV in Fig. 8) show that the A_2' transition in (I) does not obscure the A_1' transition.

As discussed in Section III, the components of $\vec{A}$ that are parallel to M (A_z, A_y) can excite A' transitions and A_x ($\perp$M) excites A" transitions, if the polarization selection rules are obeyed in Cu(211) (see Table I). Finite angular acceptance of the analyzer ($\pm 3^\circ$), angular alignment ($\pm 1^\circ$ in θ, $\pm 3^\circ$ in ϕ), and incomplete polarization of the radiation (>97 percent polarized) are among the effects which contribute to the apparent breaking of these rules; i.e., weak photoemission from A_1'' and somewhat stronger emission from A_2'' in (II), where they are both forbidden because $|A_x| = 0$ (see Fig. 2). In (I), where $|A_x|$ and $|A_z|$ are both greater than zero, the relative intensity ratio of A' to A" photoexcitation should be proportional to $|A_z/A_x|^2$ which is 3 for the incident radiation field. However, there is no A_4' peak in (I) except at higher photon energies and A_1'' typically dominates over A_2' and A_3', suggesting that $|A_z/A_x|^2$ is effectively <1. This might arise from a classical Fresnel-type

modification of the macroscopic electromagnetic field as it passes through the vacuum-solid interface.[42] Smith, et al.[43] have discussed these effects in the ARP polarization studies of Cu(111) by Knapp, et al.[2] They defined the parameter $\xi_t = \xi_t(h\nu,\theta_i) = |A_{zt}/A_{xt}|^2$ where $|A_{zt}|$ and $|A_{xt}|$ are the transmitted components of the $\vec{A}$ vector, and θ_i is the optical angle of incidence ($\theta_i = 60^\circ$ in the present case). ξ_t can be determined from ε_1 and ε_2, the dielectric constants of the sample. Using known ε_1 and ε_2 values for Cu,[44] ξ_t has been calculated in the energy range 9 eV $\leq h\nu \leq$ 34 eV and is shown in Fig. 9 (bottom curve). It is generally $<<3$ ($\xi_i = |A_{zi}/A_{xi}|^2 = 3$) throughout, and is <1 below $h\nu$ = 26 eV. This effect accounts at least qualitatively for the large observed intensity for A" states in (I).

Radiation refraction effects in our data may be discussed further. Also shown in Fig. 9 are intensity ratio curves for the s-p plateau region discussed above (energy window 0 eV $\leq -E^F \leq$ 1.8 eV) and the d bands (energy window 1.8 eV $\leq -E^F \leq$ 5.0 eV) as functions of photon energy. The ratio R_{21} is the ratio of intensity in (II) to the intensity in (I). As discussed before, the s-p region is more intense in (II) (where the A_4' transition is "most allowed") than in (I), with $R_{21}(sp) > 1$ for photon energies $h\nu > 13$ eV. The feature labeled "a" in Fig. 9 marks the energy at which the direct-transition peak from A_4' is centered in the 1.8 eV window in (II) ($E^F \sim -0.9$ eV). There is an inflection point above this, presumably because part of the A_4' direct transition has moved out of the window. The point "b" locates the energy at which the center of the A_4' direct

transition in (II) is at the edge of the window ($E^F \sim -1.8$ eV). At higher energies, the ratio drops, but it rises again from about 1.5 at $h\nu = 22$ eV to 1.8 at $h\nu = 25$ eV. The d-band ratio $R_{21}(d)$ in Fig. 9 is more striking. It is less than 1 throughout the energy region, reaching its maximum value of 0.90 at $h\nu = 18$ eV. It remains essentially flat for about 4 electron volts thereafter, then dips suddenly to 0.67 at 26 eV, then rises to a second maximum of 0.90 at 32 eV. The large dip at 26 eV (feature "c") signals a sudden relative increase in d-band emission in (I), i.e., from A_1'' and/or A_2'' states near the center of the D - X line. The peak in $R_{21}(sp)$ indicates an increase in s-p emission in (II) relative to (I). The reason for the d-band ratio fluctuation could simply be the larger density of initial states in the center of the D - X portion of the zone, where $v_g \sim 0$ for these valence bands, but there is no reason to expect the observed differential increase in photoemission in (I) on this basis because A_2', A_3', and A_4' also have $v_g \sim 0$ at these $\vec{k}_i$ values. Also, this would not explain the s-p ratio fluctuation. The explanation is more likely in the sudden drop in ξ_t (lower curve) near $h\nu = 26$ eV. The ξ_t curve dips near $h\nu = 26$ eV because ε_2 rises[44] from 0.690 at $h\nu = 23$ eV to 0.761 at $h\nu = 25$ eV. In turn, ε_2 rises primarily because of d → f electron transitions[45] occurring at or near Γ. Although ξ_t cannot quantitatively account for R_{21} over the entire energy range, its rapid variation near $h\nu = 26$ eV suggests that R_{21} is attenuated for d bands and enhanced for s-p electrons simply because of <u>enhanced</u> suppression of A_z, i.e., a relative attenuation of emission from bands

of A' symmetry and/or an enhanced A" signal in (I) takes place. The intense A" d-band emission in (I) causes $R_{21}(d)$ to drop, while the absence of s-p electrons with A" symmetry causes $R_{21}(sp)$ to increase. We note that an analysis like this is possible only as the result of the simple symmetry selection rules for Cu(211). Smith, et al.[43] required a constant value of $\xi_t \sim 0.09$ (i.e., a factor of ~5 lower than the classical Fresnel value) to obtain good agreement between their theory and the experimental data of Knapp, et al.[2] While it is difficult to compare this with our experimental results without a theoretical calculation, a factor of ~5 reduction in ξ_t (e.g., $\xi_t \sim 0.18$ at $h\nu = 20$ eV) would not seem to be warranted by R_{21} near unity over a large part of the energy range above 16 eV. Furthermore, the striking similarity in the fluctuation of the R_{21} and ξ_t curves near 26 eV suggests that ξ_t is not an energy-independent constant in this photon energy range.

Finally, it is interesting to compare EDCs for different θ_i. In Fig. 10, spectra at $h\nu = 17$ eV are shown for both orientations and θ_i = 50°, 60°, and 80° corresponding to ξ_i = 1.4, 3.0, and 32; and ξ_t = 0.52, 0.64, and 0.78, respectively. For (II), the spectra are normalized to the intensity of $(A_2' + A_3')$ (this is essentially A_2' at this energy), and (I) EDCs are normalized to the A_1'' intensity. Generally, only changes in relative peak intensities are induced by varying θ_i at all photon energies studied. New peak structures are <u>not</u> observed. For example, in (I) at 17 eV (Fig. 10), the s-p plateau, $(A_2' + A_3')$, and A_1'

grow with increasing θ_i, in consonance with the trend in $\xi_t(\theta_i)$. In (II), $|A_x| = 0$; thus, the relative intensities of the four A' peaks in (II) [A_4', (A_3' + A_2'), and A_1'] do not significantly change with θ_i. However, it was noted above that residual experimental misalignment effectively leads to $|A_x| \gtrsim 0$. Therefore, increasing θ_i in (II) suppresses the residual $|A_x|$ component in a manner similar to (I), accounting for the observed attenuation of A_2'' intensity in (II) (Fig. 10).

B. Final-State Band Structure

Previous experimental and theoretical work on low-index faces[17,24,25] showed evidence for unusual behavior in ARP when the excitation energy placed photoelectrons into bulk conduction band gaps. The main feature supporting this is a "lack of dispersion" of the initial-state bands,[25] arising because the $\vec{k}$ vector of the photoelectron is imaginary in the gap, thereby allowing only states at the surface to be excited.[17,24] Because $|\vec{k}_{\parallel}| = 0$ in normal emission, band-gap photoemission corresponds to photoexcitation from $\bar{\Gamma}$, independent of photon energy. Hence, sweeping the photon energy resulted in direct transitions with concomitant valence-band dispersion as $\vec{k}_{\perp}$ was varied across the zone, until the gap was reached.[25] However, bulk conduction band gaps along high symmetry directions invariably occur at Γ and/or zone boundaries, and it could be argued equally well that the lack of dispersion is simply a consequence of $v_g \sim 0$ for the initial-state bands. Additionally, lack of dispersion in d bands is not necessarily indicative of band-gap photoemission, because they are already reasonably flat.

As a consequence of low symmetry, the conduction band gap between A_5' and A_6' in Cu[211] occurs away from the zone boundary, where initial-state s and s-p bands (A_1' and A_4', respectively) have large group velocities. Thus, an unambiguous test of band-gap photoemission should be possible in Cu(211). The experimental dispersion relations in Fig. 7 show that there is no evidence for the band-gap photoemission process discussed previously. The portion of the band structure expected to be affected by the bulk band gap is enclosed within the vertical dashed lines. Not only do the s and s-p bands disperse throughout the gap region, but the absolute s-p and d-band intensities used to derive the R_{21} curves in Fig. 9 show no unusual structure in the spectra for either orientation. Previous work in this laboratory on low-index faces of Ag,[6] Au,[8,9] and Pt[8,14] also showed initial-state dispersion at photon energies for which the final states should be in a conduction-band gap, but the present Cu(211) work is by far the most convincing evidence for this, because of the large slope in the A_1' and A_4' bands away from the zone boundary. Furthermore, Fig. 7 shows that d-band dispersion in the gap region is minimal in both theory (interpolated bands) and experiment, indicating that a dispersionless d band is not sufficient evidence for a band-gap photoemission process.

The apparent lack of band-gap photoemission leads directly to a discussion of the final-state band structure in ARP and the success of the single-plane-wave approximation for its dispersion relation. It has been shown that the finite lifetime of the photoelectron (which is relatively short in Cu at these energies[2]) introduces an imaginary component to its $\vec{k}$ vector regardless of its position in the zone,[46]

and that the effect of this is to remove gaps in the band structure, giving rise to more free-electron-like conduction bands.[46,47] It has also been pointed out that while k-broadening is still more important in the band-gap region than outside it, the increase in the spread in $\vec{k}$ (i.e., Im $\vec{k}$) is only by a factor of 2-3.[47] Physically, damping attenuates the interaction between the photoelectron and the periodic lattice potential.[47] Since band gaps arise from Bragg scattering, it is not surprising that damping closes these gaps. Strictly speaking, all of this points to the inadequacy of the one-electron band structure picture in describing photoelectron dispersion relations.[48] The photoelectron is short-lived, and the bulk band-structure does not account for the symmetry-breaking influence of the hole, which is relatively long-lived. However, experimental[5,30] results suggest that the quasi-free-electron approximation works well over a wide range of final-state energies. The striking evidence for this in Cu(211) represents another important result of this work.

V. SUMMARY AND CONCLUSIONS

We have presented results of normal emission ARP studies using variable-energy synchrotron radiation for the stepped Cu(211) face. The photoemission process is similar to low-Miller-index faces of copper.[1,2,4] All peak structures in the EDCs, except for a previously observed DOS feature at the leading edge of the 3d bands and the s-p plateau, are shown to derive from $\vec{k}_\perp$-conserving direct transitions along the [211] direction in k-space. The presence of the stepped

surface does not introduce any other spectral features, although part of the photoemission intensity in various peaks (particularly A_2'' in orientation II) may arise from DOS photoemission. Excellent agreement between peak-energy positions and bulk-initial state dispersion relations is obtained if the final-state wavefunction is assumed to contain only one plane-wave component; i.e., no secondary Mahan emission features were found. This excellent agreement with the interpolated bulk bands suggests that any photoelectron refraction effects associated with non-normal emission, i.e., from step and/or terrace directions, are negligible. In consonance with previous work,[5,30] a quasi-free-electron parabolic final-state dispersion relation was used successfully, even at energies corresponding to a symmetry band gap near the zone boundary. The top and bottom valence bands, A_4' and A_1', are shown to disperse even when the final state falls in this gap region, suggesting that the one-electron bulk-band gap picture is not applicable to the description of photoelectron conduction-band structure. Finally, radiation polarization selection and refraction at the vacuum-solid interface are observed to play an important role in determining relative peak intensities. This is demonstrated in a particularly straightforward manner with Cu(211) because there are only two irreducible representations (A' and A") for eigenstates along the [211] direction. In fact, polarization selection greatly reduces the problem of determining individual band empirical dispersion relations along the complicated [211] direction.

These studies suggest that the stepped structure of the Cu(211) surface does not significantly perturb its bulk-like electronic structure, a result which was anticipated in previous work.[20,49] In contrast to this, it would be interesting to investigate the valence-band structure properties of stepped crystal faces of the catalytically active Group VIII metals, particularly in light of recent Pt(100)-(5x1) results,[14] which showed large DOS contributions to the normal emission EDCs for the reconstructed surface.

Based on these Cu(211) results, we conclude that bulk-valence band structure determination can be applied to low-symmetry directions in a manner analogous to the (111), (100), and (110) faces, thereby alleviating the necessity for crystal faces with a specific high-symmetry orientation. This has implications for band-structure studies of more complicated materials, where it may not be possible to obtain high-symmetry faces.

Finally, the four major results of this work are summarized: (1) it is possible to determine experimental valence-band dispersion relations for non-low-index directions; (2) valence-band dispersion relations for stepped Cu(211) show excellent agreement with bulk valence bands interpolated along the [211] direction; (3) the quasi-free electron model describes photoelectron dispersion relations, but the one-electron bulk conduction bands do not; and (4) there is no evidence for band-gap photoemission.

ACKNOWLEDGMENTS

We wish to thank K. A. Mills and J. G. Tobin for assistance in carrying out some of the photoemission measurements, and Mrs. Winifred Heppler for assisting in the preparation of the copper crystal. In addition, we acknowledge M. G. Mason for many stimulating discussions.

This work was supported by the Director, Office of Energy Research, Office of Basic Energy Sciences, Chemical Sciences Division of the U. S. Department of Energy under Contract No. W-7405-ENG-48. It was performed in part at the Stanford Synchrotron Radiation Laboratory, which is supported by the NSF Grant No. DMR 77-27489, in cooperation with the Stanford Linear Accelerator Center.

REFERENCES

1. J. Stöhr, P. S. Wehner, R. S. Williams, G. Apai, and D. A. Shirley, Phys. Rev. B 17, 587 (1978); D. A. Shirley, J. Stöhr, P. S. Wehner, R. S. Williams, and G. Apai, Physica Scripa 16, 398 (1977).
2. J. A. Knapp, F. J. Himpsel, and D. E. Eastman, Phys. Rev. B 19, 4952 (1979).
3. P. O. Nilsson and L. Ilver, Solid State Commun. 17, 667 (1975); L. Ilver and P. O. Nilsson, Solid State Commun. 18, 677 (1976).
4. P. Thiry, D. Chandesris, J. Lecante, C. Guillot, R. Pinchaux, and Y. Petroff, Phys. Rev. Lett. 43, 82 (1979).
5. Z. Hussain, S. Kono, L.-G. Petersson, C. S. Fadley, and L. F. Wagner, Phys. Rev. B 23, 724 (1981), and references therein.
6. P. S. Wehner, R. S. Williams, S. D. Kevan, D. Denley, and D. A. Shirley, Phys. Rev. B 19, 6164 (1979), and references therein; K. A. Mills, M. G. Mason, R. F. Davis, R. Watson, G. Thornton, J. G. Tobin, Z. Hussain, E. Umbach and D. A. Shirley, to be published.
7. G. V. Hansson and S. A. Flodström, Phys. Rev. B 17, 473 (1978).
8. K. A. Mills, R. F. Davis, S. D. Kevan, G. Thornton, and D. A. Shirley, Phys. Rev. B 22, 581 (1980).
9. R. F. Davis, M. G. Mason, Z. Hussain, J. G. Tobin, L. E. Klebanoff, and D. A. Shirley, to be published.
10. P. Heimann, H. Miosga, and H. Neddermeyer, Solid State Commun. 29, 463 (1979).
11. G. V. Hansson and S. A. Flodström, Phys. Rev. B 18, 1572 (1978).

12. D. E. Eastman, F. J. Himpsel, and J. A. Knapp, Phys. Rev. Lett. 40, 1514 (1978); F. J. Himpsel, J. A. Knapp, and D. E. Eastman, Phys. Rev. B 19, 2919 (1979).

13. F. J. Himpsel and D. E. Eastman, Phys. Rev. B 18, 5236 (1978).

14. G. Thornton, R. F. Davis, K. A. Mills, and D. A. Shirley, Solid State Commun. 34, 87 (1980).

15. J. F. van der Veen, F. J. Himpsel, and D. E. Eastman, Phys. Rev. B 22, 4226 (1980).

16. R. F. Davis, K. A. Mills, G. Thornton, S. D. Kevan, and D. A. Shirley, VI International Conference on Vacuum Ultraviolet Radiation Physics (Charlottesville, VA, 1980), Vol. I, pp. 1-3.

17. B. Feuerbacher and R. F. Willis, J. Phys. C 9, 169 (1976).

18. See e.g., Gabor A. Somorjai, Chemistry in Two Dimensions: Surfaces (Cornell University, Ithaca, NY, 1981), Chapter 4.

19. G. A. Somorjai, Adv. Catal. 26, 1 (1977); D. W. Blakely and G. A. Somorjai, J. Catal. 42, 181 (1976).

20. R. S. Williams, P. S. Wehner, S. D. Kevan, R. F. Davis, and D. A. Shirley, Phys. Rev. Lett. 41, 323 (1978).

21. K. Ždánský and Z. Šroubek, J. Phys. F 6, L205 (1976).

22. M. C. Desjonquères and F. Cyrot-Lackmann, Solid State Commun. 18, 1127 (1976).

23. Y. W. Tsang and L. M. Falicov, J. Phys. C 9, 51 (1976).

24. Peter J. Feibelman and D. E. Eastman, Phys. Rev. B 10, 4932 (1974); F. J. Himpsel, Appl. Opt. 19, 3964 (1980).

25. E. Dietz and F. J. Himpsel, Solid State Commun. 30, 235 (1979).

26. We used a solution of sodium 2-mercaptobenzimidazole-5-sulfonate and polyethylene glycol 400 in HCl; see J. S. Ahearn, J. P. Monaghan, and J. W. Mitchell, Rev. Sci. Instrum. 41, 1853 (1970).

27. B. Lang, R. Joyner, and G. A. Somorjai, Surf. Sci. 30, 440 (1972); 454 (1972).

28. S. D. Kevan and D. A. Shirley, Phys. Rev. B 22, 542 (1980).

29. G. D. Mahan, Phys. Rev. B 2, 4334 (1970).

30. See e.g., R. S. Williams, P. S. Wehner, J. Stöhr, and D. A. Shirley, Surf. Sci. 75, 215 (1978); Refs. 1, 6, 8, 9, 14, and 16.

31. N. V. Smith, Phys. Rev. B 3, 1862 (1971).

32. L. Hodges, H. Ehrenreich, and N. D. Lang, Phys. Rev. 152, 505 (1966).

33. J. F. Janak, A. R. Williams, and V. L. Moruzzi, Phys. Rev. B 11, 1522 (1975).

34. Glenn A. Burdick, Phys. Rev. 129, 138 (1963).

35. J. Hermanson, Solid State Commun. 22, 9 (1977).

36. F. J. Himpsel, Appl. Opt. 19, 3964 (1980), and references therein.

37. P. O. Gartland, S. Berge, and B. J. Slagsvold, Physica Norvegica 7, 39 (1973).

38. S. Andersson, Surf. Sci. 18, 325 (1969).

39. M. R. Halse, Phil. Trans. Roy. Soc. A 265, 507 (1969).

40. M. Lax and J. J. Hopfield, Phys. Rev. 124, 115 (1961).

41. See e.g., L. F. Ley, J. Electron Spectroscopy 15, 329 (1979).

42. J. A. Stratton, Electromagnetic Theory (McGraw-Hill, New York, 1941), Chapter IX.

43. N. V. Smith, R. L. Benbow, and Z. Hurych, Phys. Rev. B 21, 4331 (1980).

44. H.-J. Hagemann, W. Gudat, and C. Kunz, J. Opt. Soc. Am. 65, 742 (1975), and Ref. 1 therein.

45. D. Beaglehole and B. Thiéblemont, Il Nuovo Cimento 39B, 477 (1977), and references therein.

46. J. B. Pendry, Surf. Sci. 57, 679 (1976); Low Energy Electron Diffraction (Academic Press, New York, 1974).

47. P. O. Nilsson and N. Dahlbäck, Solid State Commun. 29, 303 (1979).

48. P. O. Nilsson, J. Kanski, and C. G. Larsson, Solid State Commun. 36, 111 (1980).

49. G. S. Painter, P. J. Jennings, and R. O. Jones, J. Phys. C 8, L199 (1975).

Table I. Polarization selection rules for normal photoemission from (211) faces of FCC crystals.[a]

Coordinate Axes			Irreducible Representations	Final State Symmetry	Allowed Initial Symmetries		
x	y	z			A_x	A_y	A_z
$[01\bar{1}]$	$[\bar{1}11]$	[211]	A' A" [b]	A'	A"	A'	A'

[a]The photoelectron propagation direction defines the z-axis in each case.

[b]Since the [211] axis in momentum space has no special symmetry designation, the symbols A' and A" chosen to represent the even and odd states, respectively, are those for the usual C_s symmetry classification.

Table II. Values of empirical valence bands along [211] in copper.

$\vec{k}_i$(units of $2\pi/a$)		Energy, $-E^F$ (eV)					
k_x	$k_y=k_z$	A_1'	A_2'	A_3'	A_1''	A_2''	A_4'
-0.12	-0.56		3.89			2.41	
-0.08	-0.54		3.84			2.56	0.00
-0.04	-0.52	4.22	3.86	3.69	2.86	2.51	0.35
0	-0.50	4.38	3.97	3.77	2.94	2.49	0.67
0.04	-0.48	4.58	3.96	3.77	3.00	2.45	0.96
0.08	-0.46	4.79	3.86	3.69	3.14	2.39	1.33
0.12	-0.44	5.05	3.77	3.62	3.27	2.34	1.66
0.16	-0.42	5.18	3.68	3.58	3.41	2.33	1.91
0.20	-0.40	5.29	3.59	3.50	3.45	2.31	2.15
0.24	-0.38	5.36	3.52	3.39	3.49	2.30	2.36
0.28	-0.36	5.39	3.43	3.31	3.52	2.36	2.52
0.32	-0.34	5.40	3.40	3.27	3.51	2.39	2.63
0.36	-0.32	5.39	3.41		3.48	2.37	2.65
0.40	-0.30		3.45		3.42	2.32	2.59
0.44	-0.28		3.58		3.33	2.23	2.48

Table III. Deviations between experimental and theoretical valence bands along [211] in copper.

Deviation Parameter, ΔE[a]	Magnitude for Valence Bands Along [211] (eV)						Overall Theoretical ΔE[b]
	A_1	A_2	A_3	A_1''	A_2''	A_4	
$\overline{\Delta E}$	0.11	0.04	0.06	0.01	0.06	0.20	0.09
ΔE_{rms}[c]	0.10	0.05	0.06	0.11	0.10	0.14	0.11
$\lvert\Delta E\rvert_{max}$[d]	0.29	0.10	0.11	0.24	0.21	0.32	0.37

[a] $\Delta E_i = E^F(\text{expt.}) - E^F(\text{int.})$; i refers to $\vec{k}_i$ from Table II.

[b] From comparison of interpolation scheme with Burdick's bands (Ref. 34) in copper, at 89 $\vec{k}_i$ points in the Brillouin zone; taken from Ref. 32.

[c] ΔE_{rms} = root-mean-square deviation.

[d] $\lvert\Delta E\rvert_{max}$ = maximum deviation.

FIGURE CAPTIONS

Fig. 1. A segment of an ideal Cu(S)-[3(111)x(100)] surface, showing three-atom terraces of (111) orientation separated by monatomic steps of (100) orientation. The $(01\bar{1})$ mirror plane cuts through the surface perpendicular to the atomic rows.

Fig. 2. Experimental geometries employed: (a) orientation I, with the plane of incidence $\perp$ to the $(01\bar{1})$ mirror plane M; (b) orientation II, with the plane of incidence $\parallel$ to M. The majority of spectra were recorded with θ_A, the angle between the surface normal $\vec{n}$ and the incident radiation vector potential $\vec{A}$, equal to 30°.

Fig. 3. Selected normal photoemission spectra for Cu(211) with photon energies in the range 9 eV $\leq h\nu \leq$ 32 eV and $\theta_A = 30°$. The spectra in panel (a) were collected with the orientation I geometry, while those in (b) were recorded with orientation II.

Fig. 4. Plot of experimental peak position versus photon energy for each structure in the Cu(211) EDCs for $\theta_A = 30°$: (a) orientation I; (b) orientation II. Open and filled circles designate weak and strong features, respectively, and the connecting lines have no theoretical significance. The plots are labelled with the appropriate initial states involved in direct transitions (vide infra).

Fig. 5. The $(01\bar{1})$ mirror plane, showing the region of k-space in the first Brillouin zone along the [211] direction (dashed lines). The points B and D, both at the zone boundary, are separated by an umklapp with $\vec{G} = (\bar{1},\bar{1},\bar{1})\ 2\pi/a$. The vector $\vec{k}_{DX}$, ending at a general point along the D - X line, is thus not actually in the [211] direction in the reduced zone scheme.

Fig. 6. The band structure of Cu interpolated along the [211] direction. The energy bands are symmetric about X, and the unoccupied bands are shown up to $E^F = 30$ eV. The bands are labeled by A' and A" irreducible representations. The A' symmetry final-state band that carries photocurrent in the [211] direction is highlighted by dashed lines in the bulk band-gap region and solid lines with filled circles elsewhere.

Fig. 7. Empirical [symbols: (•) A_1', A_2', A_4', DOS; (◇) A_3'; (○) A_1''; and (□) A_2''] and theoretical (solid lines, from interpolated bands in Fig. 6) valence-band dispersion relations for Cu(211). A partial photon energy scale is indicated at E_F, and the vertical arrows are from de Haas van Alphen data (Ref. 39). The dashed vertical lines bracket the region for which the $\vec{k}$-vectors lie in the bulk conduction band gap.

Fig. 8. A direct comparison of photoemission spectra at selected photon energies for both orientations, with $\theta_A = 30°$, showing a strong dependence on radiation polarization orientation. The structures are labeled by the appropriate bands involved in direct transitions.

Fig. 9. Intensity ratio $R_{21} = \mathcal{I}(II)/\mathcal{I}(I)$ versus photon energy for s–p electron intensity [$R_{21}(sp)$, upper curve] and d-band electrons [1.6 x $R_{21}(d)$ shown, middle curve]. The energy windows for the ratio curves are indicated in the lower right corner, and the labels a, b, and c are discussed in the text. Also shown is a plot of the parameter $\xi_t = |A_{zt}/A_{xt}|^2$ versus photon energy for copper, where $|A_{zt}|$ and $|A_{xt}|$ are the transmitted components of the radiation vector potential.

Fig. 10. A direct comparison of photoemission spectra at $h\nu = 17$ eV and various values of the angle of incidence θ_i, for both orientations. The direct-transition peak positions are indicated on the horizontal axis.

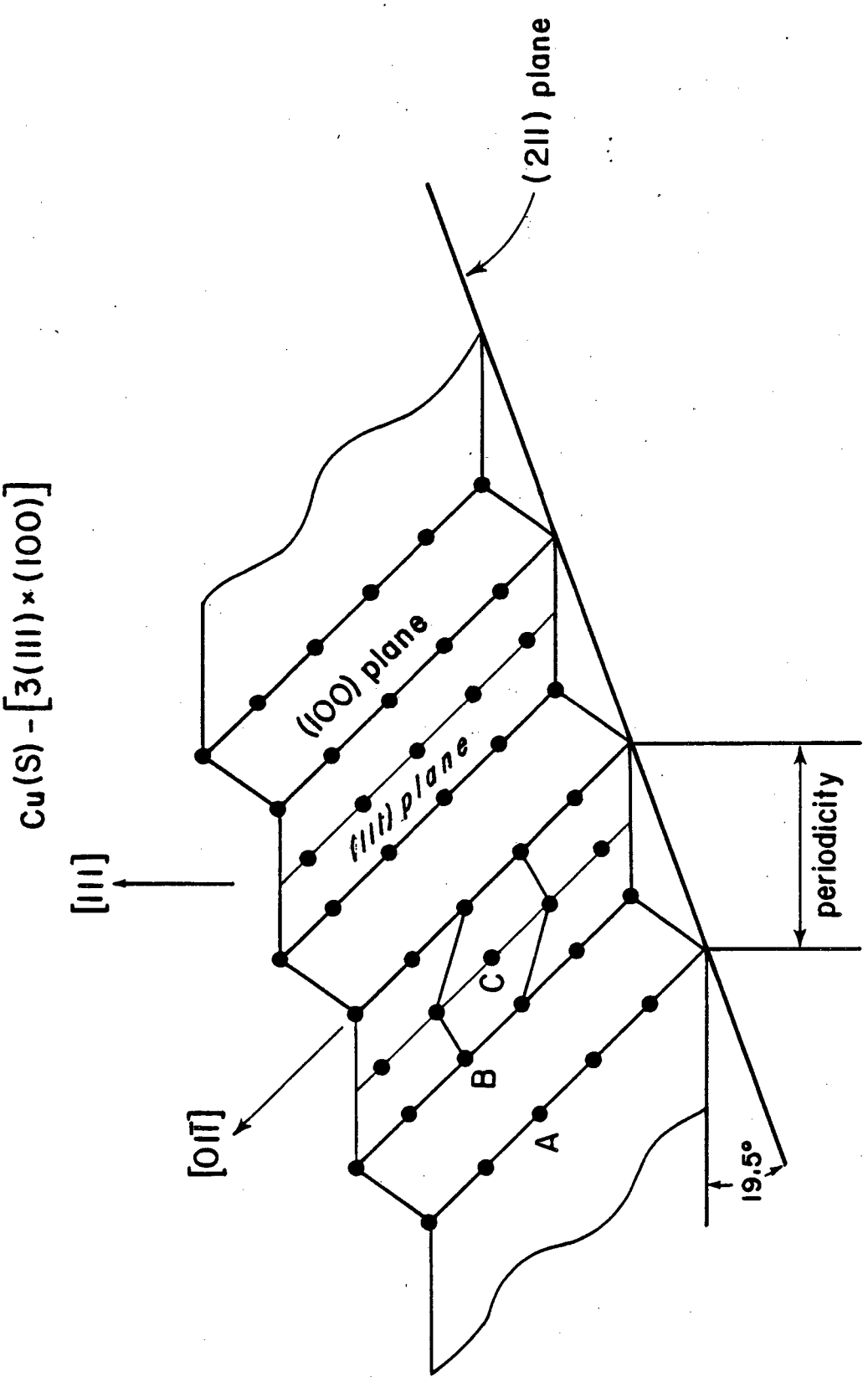

XBL 7610-4160

Figure 1

(a) Orientation I

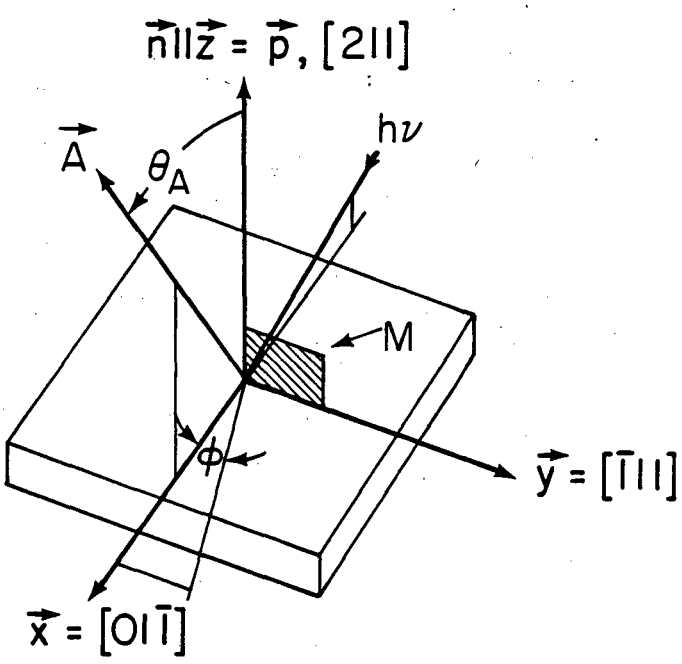

(b) Orientation II

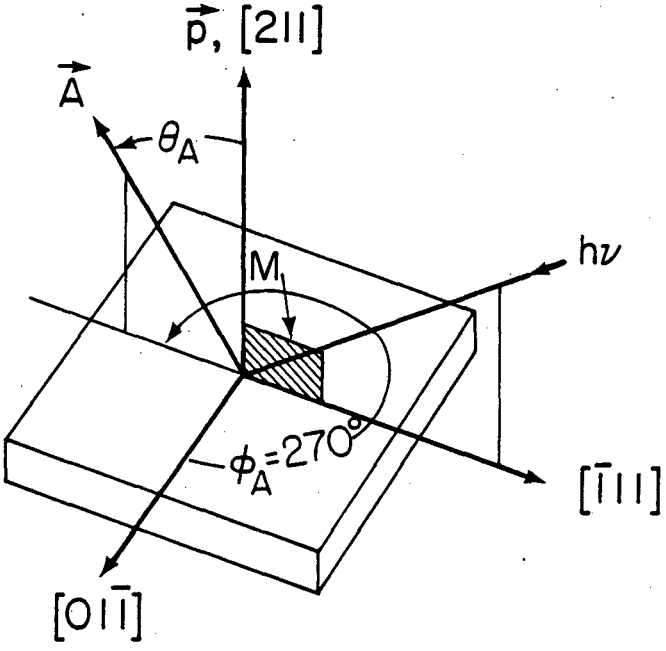

XBL 817-2379

Figure 2

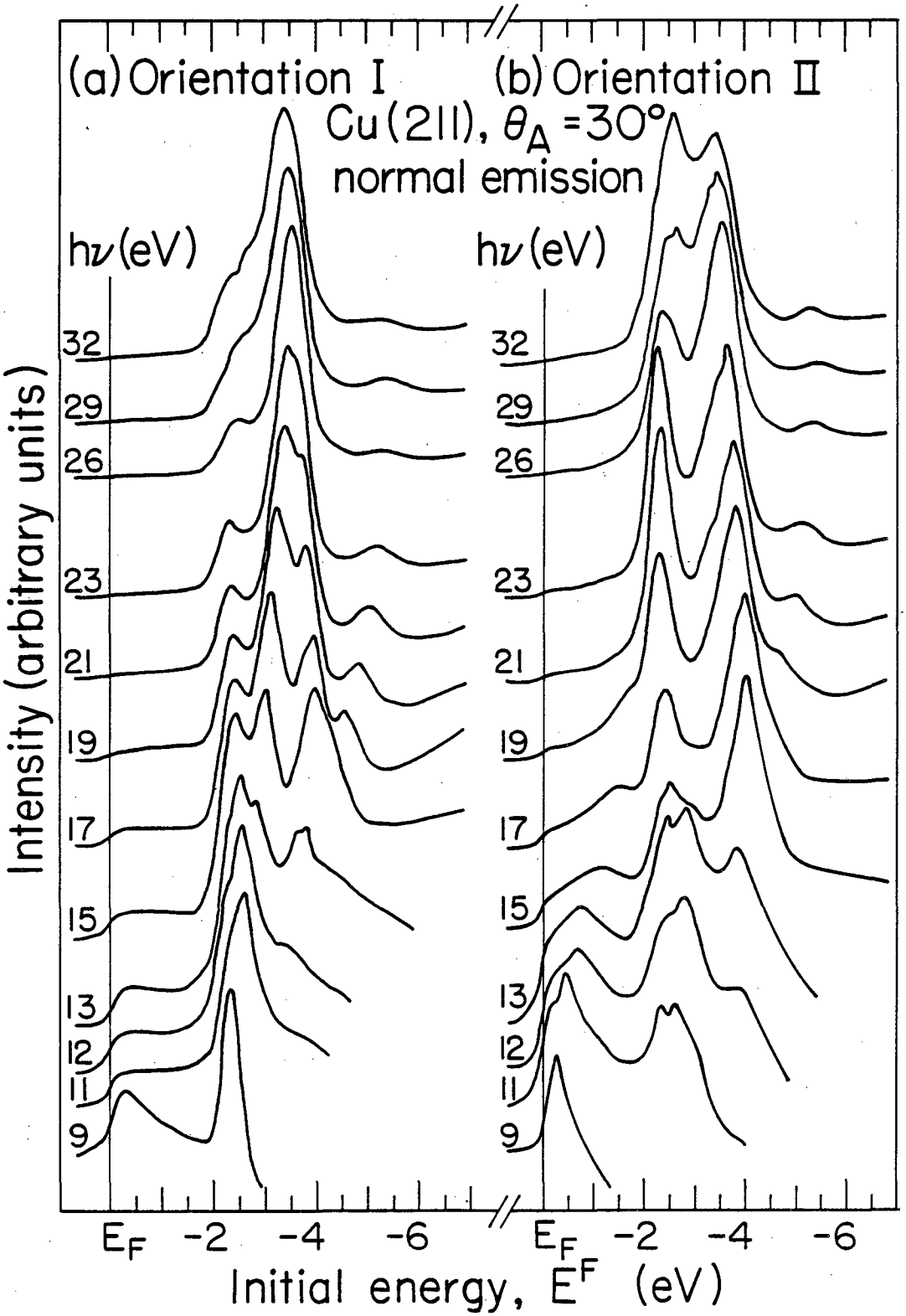

XBL 817-2377

Figure 3

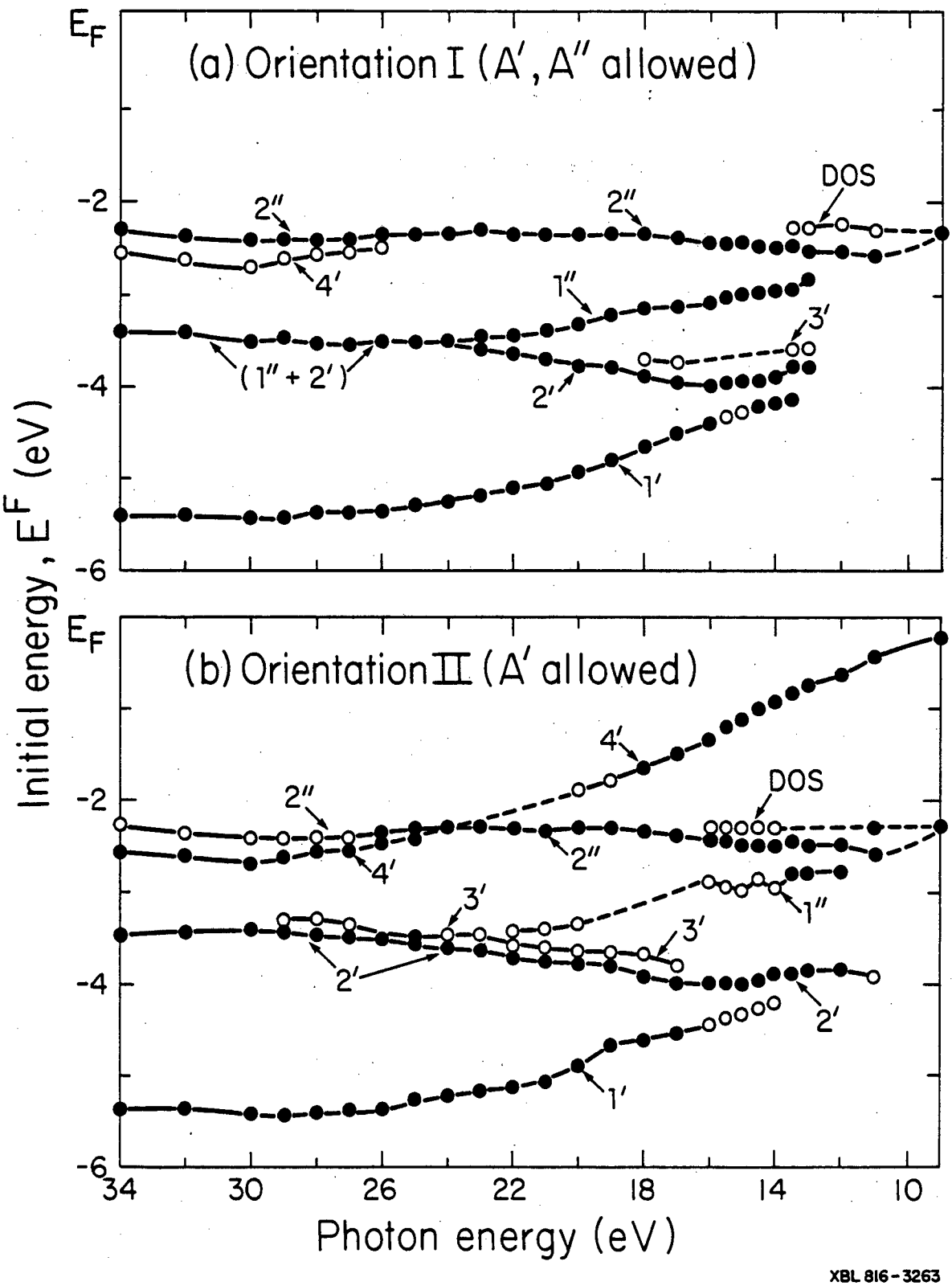
(a) Orientation I (A′, A″ allowed)
(b) Orientation II (A′ allowed)
E_F
DOS
2″
4′
1″
3′
(1″ + 2′)
2′
1′
Initial energy, E^F (eV)
-2
-4
-6
34
30
26
22
18
14
10
Photon energy (eV)
XBL 816-3263

Figure 4

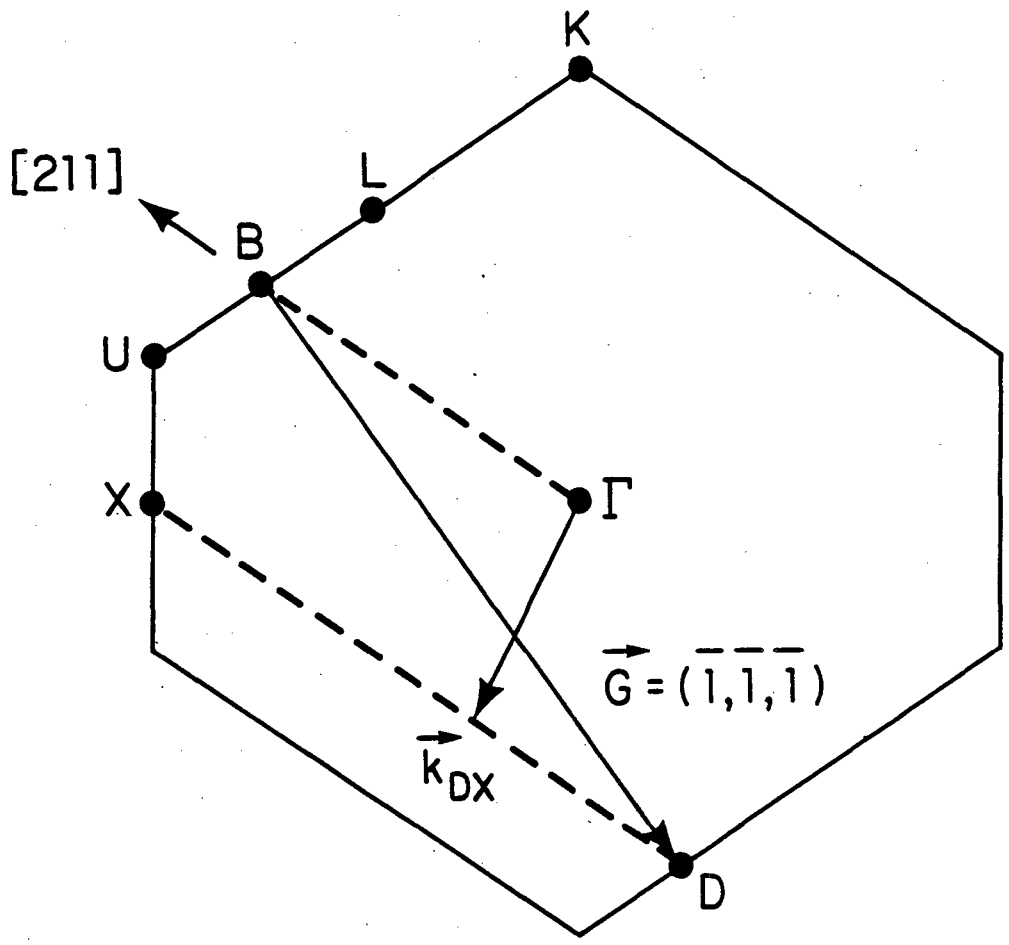
K
[211]
L
B
U
X
Γ
$\vec{G} = (\bar{1},\bar{1},\bar{1})$
$\vec{k}_{DX}$
D
(0$1\bar{1}$) projection
XBL816-3262

Figure 5

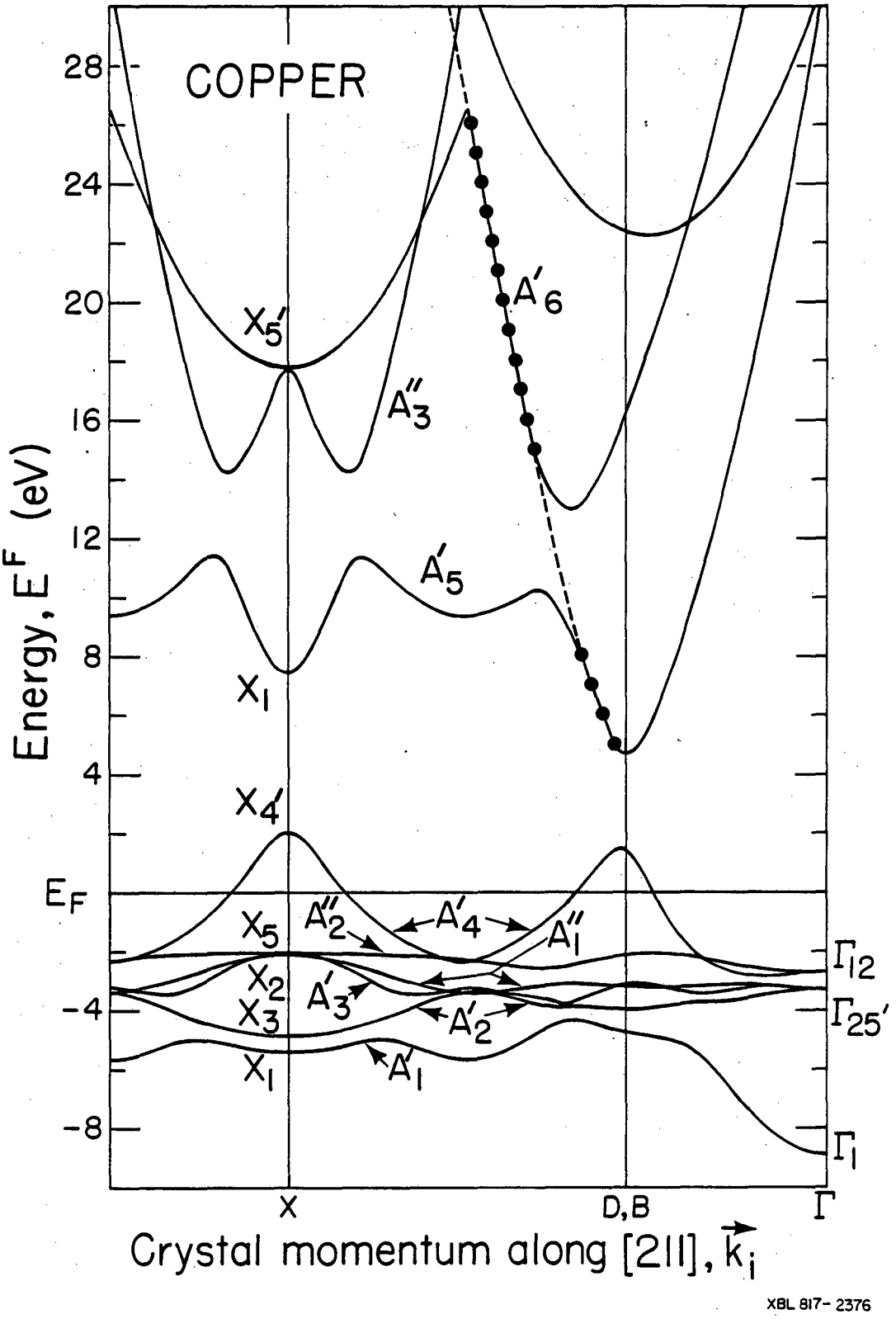
COPPER
28
24
20
16
12
8
4
-4
-8
Energy, E^F (eV)
E_F
X_5'
A_3''
A_6'
A_5'
X_1
X_4'
X_5
A_2''
A_4'
A_1''
X_2
X_3
A_3'
A_2'
X_1
A_1'
Γ_{12}
$\Gamma_{25'}$
Γ_1
X
D,B
Γ
Crystal momentum along [211], $\vec{k}_i$
XBL 817-2376

Figure 6

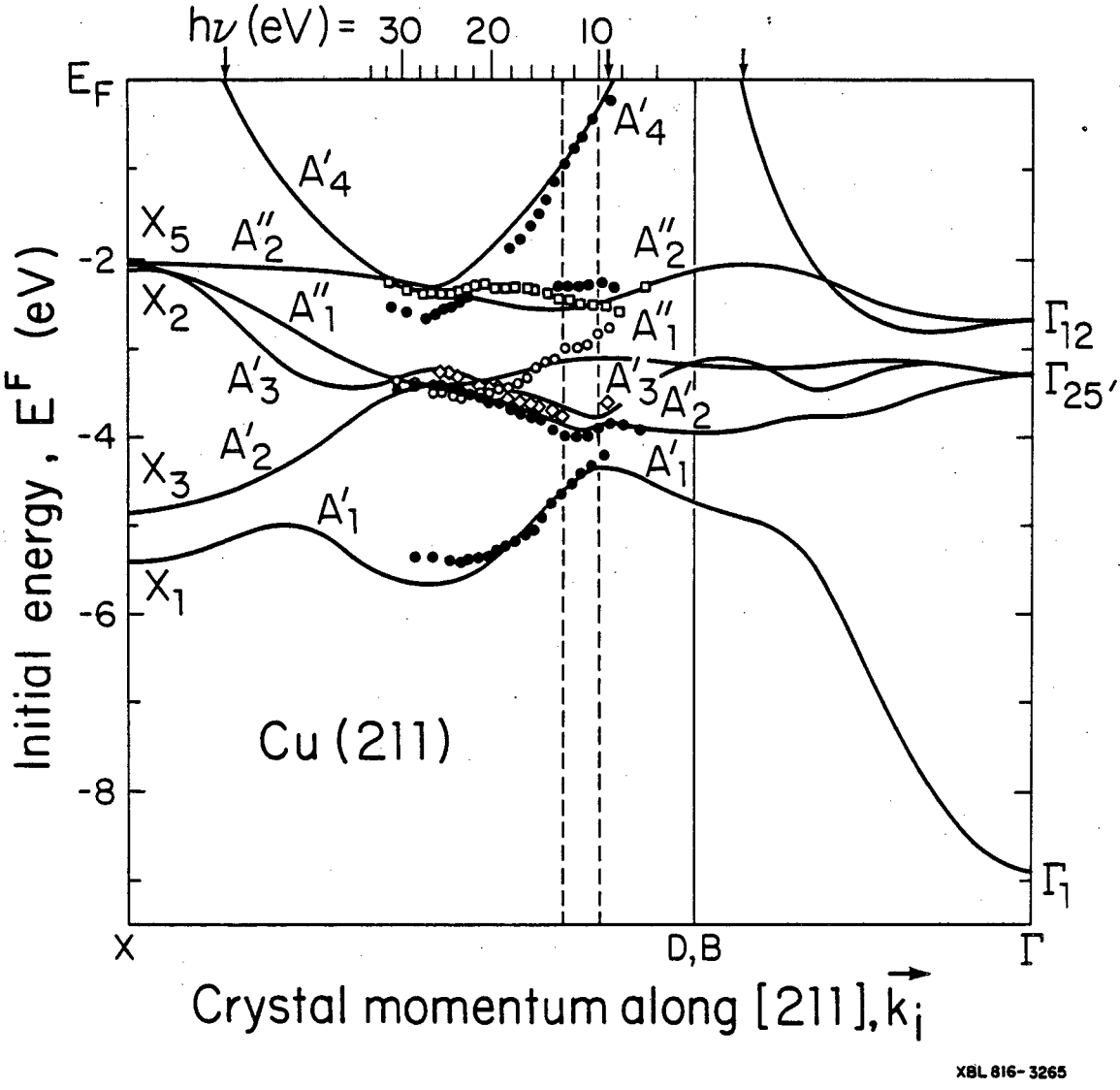
hν (eV) = 30 20 10
E_F
-2
-4
-6
-8
Initial energy, E^F (eV)
X_5
X_2
X_3
X_1
A''_2
A''_1
A'_4
A'_3
A'_2
A'_1
Cu (211)
Γ_12
Γ_25'
Γ_1
X
D,B
Γ
Crystal momentum along [211], k_i
XBL 816-3265

Figure 7

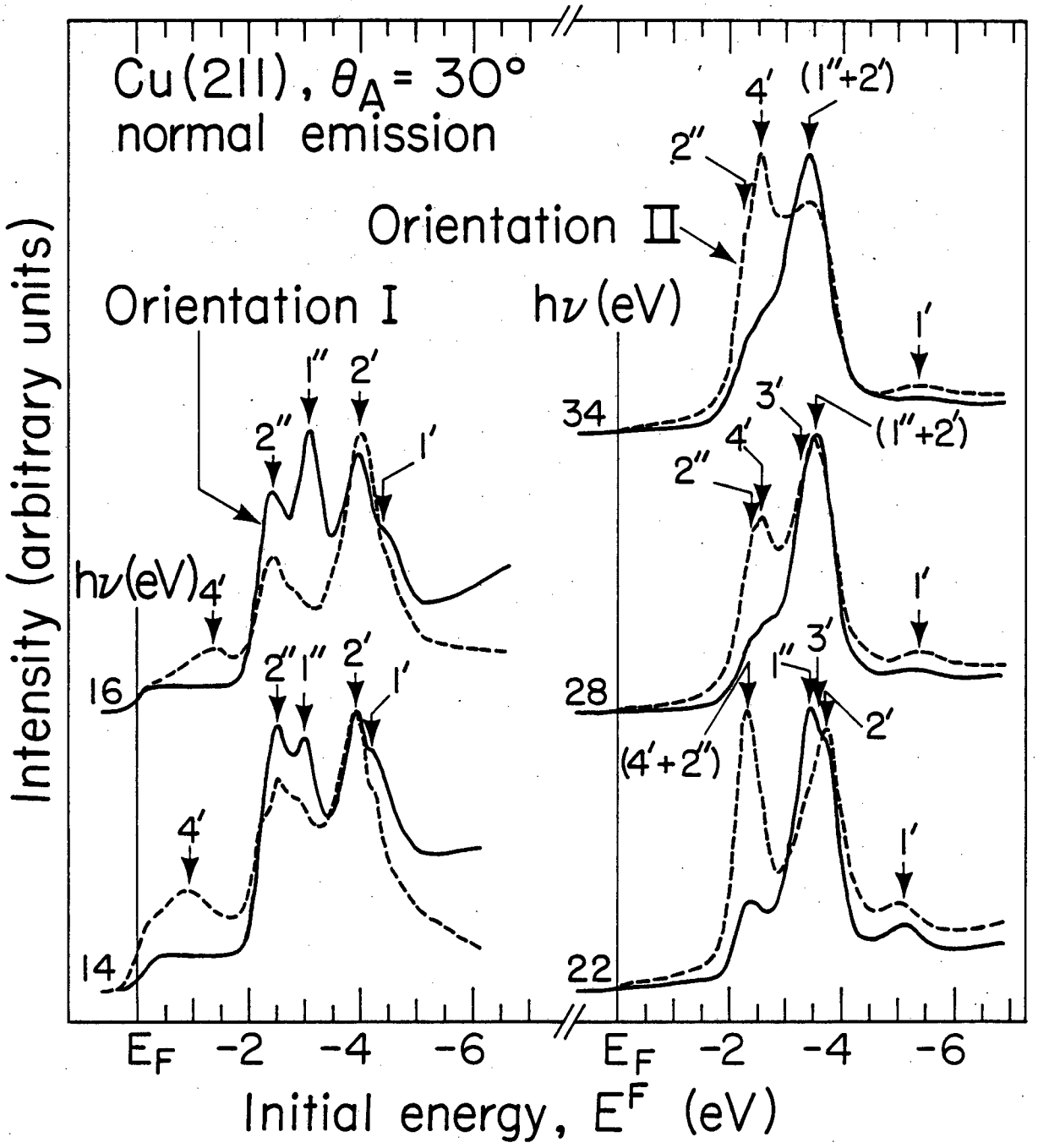

XBL 817-2378

Figure 8

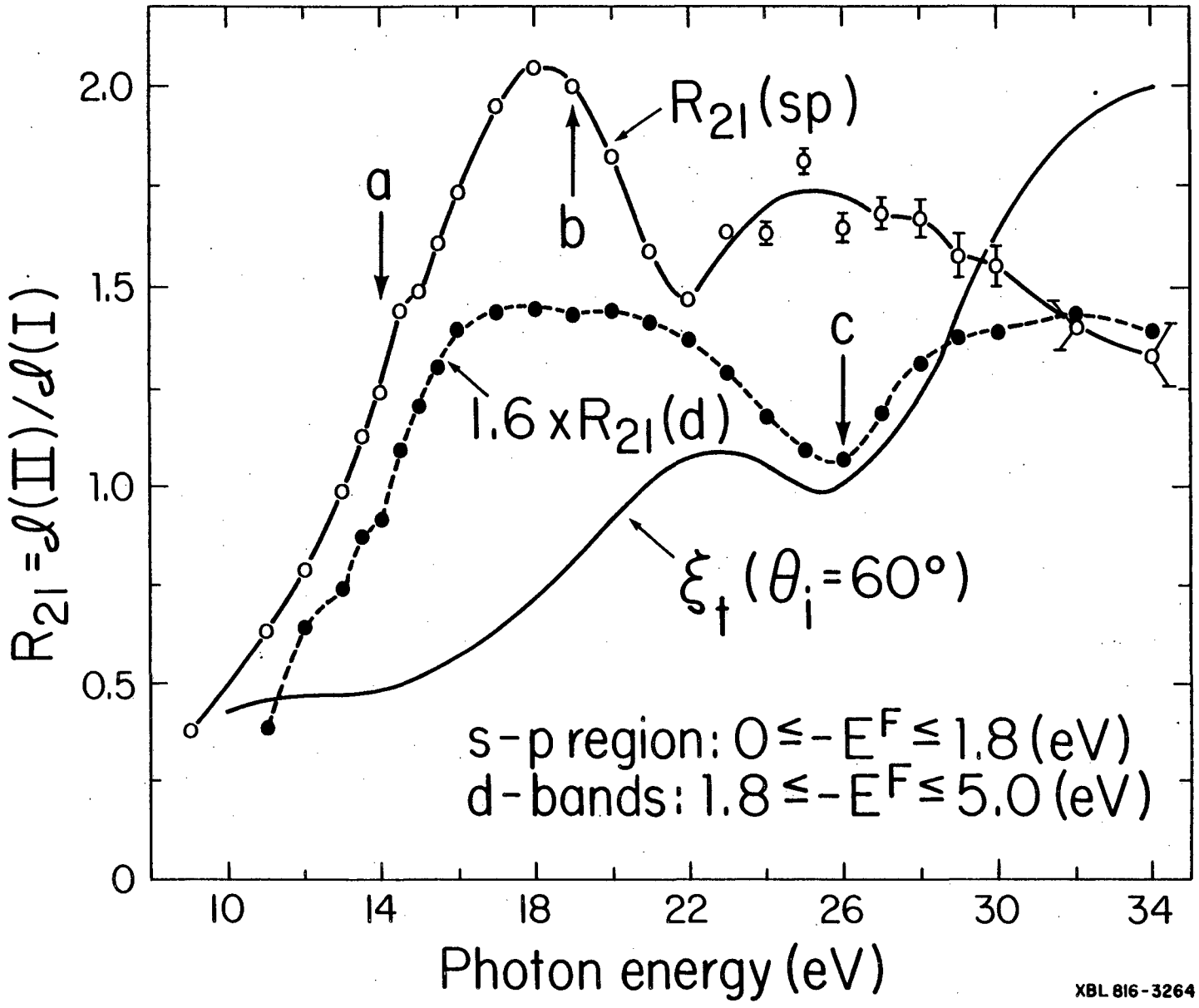
2.0
1.5
1.0
0.5
0
10
14
18
22
26
30
34
$R_{21} = \mathcal{J}(II)/\mathcal{J}(I)$
Photon energy (eV)
$R_{21}(sp)$
a
b
c
$1.6 \times R_{21}(d)$
$\xi_t(\theta_i = 60°)$
s-p region: $0 \leq -E^F \leq 1.8$ (eV)
d-bands: $1.8 \leq -E^F \leq 5.0$ (eV)
XBL 816-3264

Figure 9

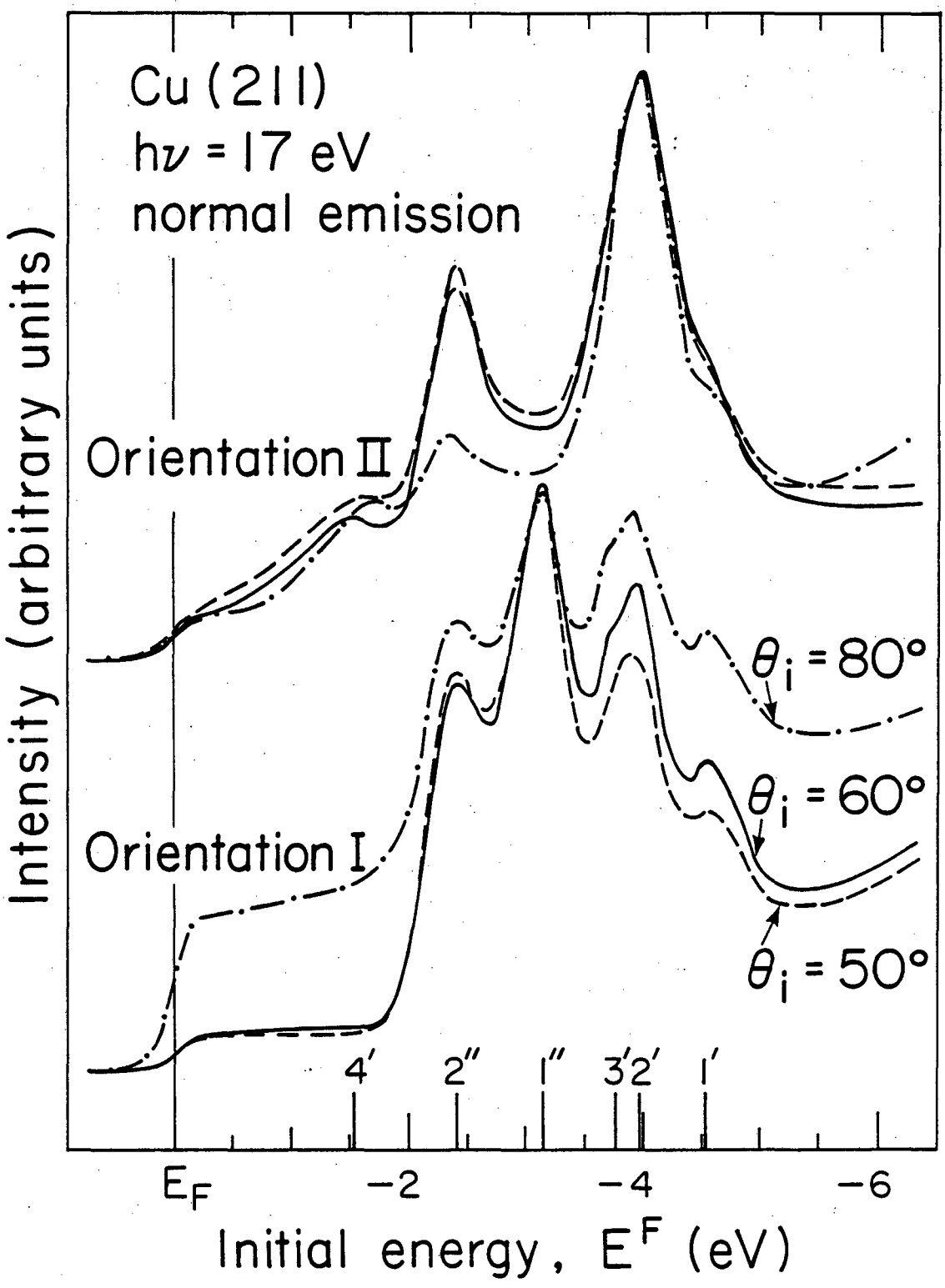

XBL 817-2381

Figure 10

This report was done with support from the Department of Energy. Any conclusions or opinions expressed in this report represent solely those of the author(s) and not necessarily those of The Regents of the University of California, the Lawrence Berkeley Laboratory or the Department of Energy.

Reference to a company or product name does not imply approval or recommendation of the product by the University of California or the U.S. Department of Energy to the exclusion of others that may be suitable.

TECHNICAL INFORMATION DEPARTMENT
LAWRENCE BERKELEY LABORATORY
UNIVERSITY OF CALIFORNIA
BERKELEY, CALIFORNIA 94720